Dual-Wavelength Hybrid Optoacoustic-Ultrasound Biomicroscopy for Functional Imaging of Large-Scale Cerebral Vascular Networks

Johannes Rebling[1,2], Héctor Estrada[1], Sven Gottschalk[1], Gali Sela[1], Michael Zwack[1], Georg Wissmeyer[1,2], Vasilis Ntziachristos[1,2] and Daniel Razansky[1,2,]*

[1]Institute for Biological and Medical Imaging (IBMI), Helmholtz Center Munich, 85764 Neuherberg, Germany
[2]Faculty of Medicine and Faculty of Electrical Engineering, Technical University of Munich, 80333 München, Germany

Key words: photoacoustics, microscopy, brain, cerebral, blood vessels, ultrasound

A critical link exists between pathological changes of cerebral vasculature and diseases affecting brain function. Microscopic techniques have played an indispensable role in the study of neurovascular anatomy and functions. Yet, investigations are often hindered by sub-optimal trade-offs between the spatiotemporal resolution, field-of-view and type of contrast offered by the existing optical microscopy techniques. We present a hybrid dual-wavelength optoacoustic biomicroscope capable of rapid transcranial visualization of large-scale cerebral vascular networks. The system offers 3D views of the morphology and oxygenation status of the cerebral vasculature with single capillary resolution and a field of view exceeding 6x8 mm², thus covering the entire cortical vasculature in mice. The large-scale optoacoustic imaging capacity is complemented by simultaneously acquired pulse-echo ultrasound biomicroscopy scans of the mouse skull. The new approach holds great potential to provide better insights into cerebrovascular function and facilitate efficient studies into neurological and vascular abnormalities of the brain.
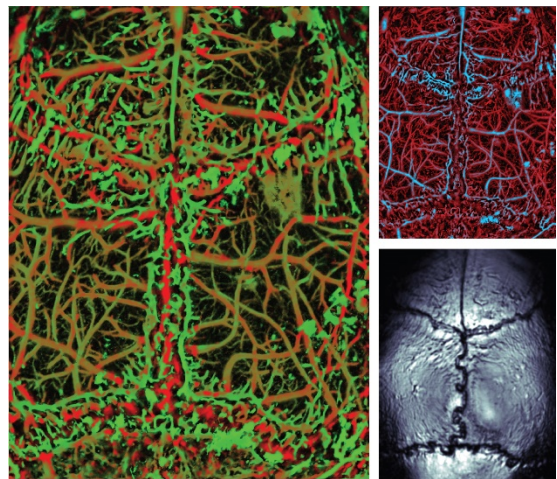
Large-scale morpho-functional optoacoustic and ultrasound imaging.

1. Introduction

Many diseases affecting neurological functions can be linked to pathological alterations of the cerebral vasculature. Some of the alterations are known to cause the disease, support and accelerate its spread , while in many other cases the interaction between the disease etiology and vascular pathology is only poorly understood, as in the case of Alzheimer's disease.[1-3] This critical link between vascular changes and disease is increasingly targeted by pre-clinical studies in mouse models mimicking the pathological changes in human cerebrovasculature.[4]

Imaging techniques, such as positron emission tomography (PET), single-photon emission computed tomography (SPECT) and functional magnetic resonance imaging (fMRI) are commonly used to provide metabolic and functional brain images in humans.[5-7] However, they lack the required micron-scale spatial resolution, necessitate exogenous contrast agents and are generally costly. Various intravital techniques, such as confocal and two-photon microscopy, optical coherence tomography or functional ultrasound (US), enable *in-vivo* imaging with sufficient spatial resolution to visualize activity in single cells and capillaries and allow for three–dimensional (3D) interrogation of the microvasculature in small animal brains.[8-10] Nevertheless, exogenous contrast agents are required for imaging oxygenation parameters with those techniques, while other limitations stem from their invasive nature and/or limited field-of-view (FOV).

Optoacoustic (OA) imaging techniques have recently provided unprecedented insights into the deep-tissue anatomy and physiology of animal model organisms due to the unique combination of rich and endogenous optical

---

* Corresponding author: dr@tum.de

absorption contrast and weak scattering of US waves in biological tissues.[11, 12] Label-free OA tomography and acoustic-resolution microscopy have enabled long-term studies in living model organisms at centimetre-scale depths and have successfully been applied for deep brain imaging in zebrafish and mice.[13-15] Optical-resolution OA microscopy has further offered high spatial resolution in visualizing finest capillaries and sub-cellular structures as well as label-free mapping of oxygen saturation dependent absorption of oxy- and deoxyhemoglobin in the murine brain.[16, 17]

Imaging performance yet greatly differs among the different OA microscopy systems. For instance, a design based on a two-axis galvo-scanner has attained B-scan speed in the 1 mm/s range while additional depth scanning was necessary for rendering 3D image volumes due to the shallow optical focus.[18] A fast voice-coil scanning system was alternatively used to attain an extended lateral FOV and higher imaging speed, whereas the effective FOV in the depth direction was similarly limited by the high-NA focusing optics and reduced detection sensitivity due to the use of an optical-acoustic beam combiner.[19] Additional performance limitations stem from the lack of high pulse repetition frequency (PRF) lasers with wavelength tuning capacity essential for spectroscopic differentiation of the blood oxygen saturation. This has been partially overcome by employing two separate laser sources at 532 nm and 559 nm running at PRF of 30 kHz, which have enabled simultaneous extraction of vascular anatomy, oxygen saturation, and blood flow. [20] The relatively slow PRF has nevertheless limited the maximum B-scan speed to about 1 mm/s, resulting in slow mechanical scanning and long image acquisition times. By employing two 100 kHz repetition lasers with different pulse durations and exploiting the difference between saturation of the OA signal by oxy- and deoxy-hemoglobin, fast MEMS-based functional OA microscopy has been recently demonstrated.[21] However, the employed saturation-based approach required high light fluence levels at the optical focus, greatly exceeding the *in-vivo* safety limits and potentially causing RBC damage.[22] In addition, the FOV in this study was limited to 3x3 mm² and the strong optical focus resulted in a narrow focal depth of less than 150 µm (calculated as the Rayleigh length), requiring both tiling in the lateral plane as well as depth scanning to image the entire cortical vasculature in 3D. The presented design furthermore relied on a highly customized water-immersible MEMS scanner, which is not readily available. The latter was replaced by a conventional galvanometer mirror in a non-conducting liquid, the design yet suffering from a similarly limited FOV and shallow depth-penetration. [23]

To address these unmet challenges, we present a fast functional OA microscopy method that uses a Pockels-cell-based wavelength switching for rapid acquisition of the spectral data. The microscope is based on a coaxial alignment of the optical and acoustic foci within a fast moving scan-head, which features a low-NA optical focus for extended imaging depth and a rapid 3D image acquisition over large lateral FOV covering an entire mouse cortex. The system is furthermore capable to simultaneously image in US pulse-echo mode, allowing for an extraction of additional anatomical data of the murine skull.

2. Materials and Methods

2.1. Optoacoustic Biomicroscopy Setup

A schematic diagram of the biomicroscope is shown in **Figure 1**, with an overview of the dual-wavelength optics displayed in Figure 1a and an illustration of the fast scan head shown in Figure 1b. The core of the microscope is formed by an optical system that enables rapid wavelength switching in combination with a fast-moving scan head sampling the specimen in epi-illumination mode. Fast switching (up to 10 kHz) between 532 nm wavelength (close to the isosbestic point of hemoglobin at 529 nm) and a second wavelength tunable in the 565-595nm range is used for spectral unmixing of the oxygen saturation.[17, 24] Linearly polarized light with a wavelength of 532 nm is generated by a Q-switched, diode end-pumped Nd:YAG laser (10 ns pulse length, model: IS8II-E, EdgeWave, Würselen, Germany). The pumping wavelength is either directly coupled into a single-mode, large mode area photonics crystal fiber (PCF, model: LMA-20, NKT Photonics, Birkerød, Denmark) or first guided into a dye laser (Credo, Sirah Lasertechnik, Grevenbroich, Germany, using a Pyrromethene 597 dye) for generating a second wavelength tunable in the 570-610 nm range. Switching between the two wavelengths is achieved by combination of a Pockels cell (PC, model: PC12SR-532, Eksma Optics, Vilnius, Lithuania) and a polarizing beam splitter (PBS, model: 420-1254HT, Eksma Optics, Vilnius, Lithuania). When activated, the PC rotates the linearly polarized 532 nm light by 90°, thus enabling its transmission by the PBS into the dye laser. In contrast, the 532 nm light is reflected by the PBS when its polarization is not altered by an inactive PC.
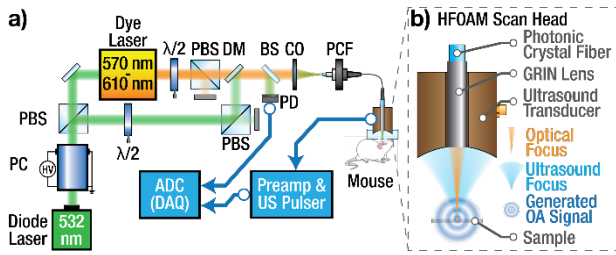
Figure 1 (a) Schematic diagram of the dual-wavelength hybrid biomicroscopy system. Both 532 nm and 578 nm pulsed laser light is coupled into a photonic crystal fiber (PCF) terminating in the fast-moving scan head, which records both the optoacoustic and pulse-echo ultrasound responses. PC = Pockels cell, PBS - polarizing beam splitter, λ/2 - half-wave plate, DM - dichroic mirror, BS - beam sampler, CO - collimating lens, ADC - analog-to-digital converter, DAQ - data acquisition card. (b) Drawing of the scan head featuring a coaxial alignment of the optical and acoustic foci for hybrid imaging.

The pulse energy of both the 578 nm and the 532 nm paths can be adjusted by means of a half-wave plate (AHWP10M-980 for 532 nm, WPH10M-532 for 578 nm, Thorlabs, Newton, USA) and an additional PBS (PBS25-532-HP for 532 nm, PBS251 for 578 nm, Thorlabs, Newton, USA) in each beam path, which allows the precise adjustment of the average pulse energies for both wavelengths. Both wavelengths are combined by a dichroic mirror (DMLP550, Thorlabs, Newton, USA) and coupled into the PCF by an achromatic lens (AC254-100-A, Thorlabs, Newton, USA). The distal end of the PCF terminates in a gradient-index (GRIN) lens (GRINTECH, Jena, Germany) which focuses the excitation light at a distance of 6.5 mm from the fiber end, as shown in Figure 1b. The GRIN lens is mounted inside an opening in the center of a custom-made, spherically focused pVDF-based US detector having an ultrawideband frequency response extending beyond 35 MHz (Precision Acoustics, Dorchester, United Kingdom). The optical and acoustic foci are aligned coaxially and confocally without the need for an optical-acoustic beam combiner [19], resulting in an optimized detection sensitivity. For volumetric imaging, the scan-head is rapidly oscillated along the x-axis by means of a fast piezostage (M-683, PI, Karlsruhe, Germany) while a second linear stage (LTM 60F-25 HSM, OWIS, Staufen, Germany) moves slowly and continuously along the y-axis, thus sampling the imaging target in a zigzag pattern. Optoacoustic A-scans are recorded by the US transducer and amplified by an 8 dB pre-amplifier (Precision Acoustics, Dorchester, United Kingdom) and a 24 dB low-noise amplifier (ZFL-500LN, Mini-Circuits, New York, USA) before they are digitized by a two-channel, 250 MS/s, 14-bit data acquisition card (M3i.4142, Spectrum Systementwicklung Microelectronic, Grosshansdorf, Germany). Pulse-echo US recording are performed using a pulser-receiver (5073PR, Olympus, Massachusetts, USA) and the same data acquisition chain. The precise position of the fast

scanning stage (x-axis) is measured in real-time during the scan using a laser distance sensor (M11L/10, MEL Mikroelektronik GmbH, Eching, Germany), whose readings are sampled by a second DAQ card (NI PCIe-6321, National Instruments, Austin, USA) and converted into stage position values using a look-up table. The latter is based on an initial slow calibration with a build-in stage encoder. The position of the slowly and continuously moving stage (y-axis) is calculated based on the known acceleration and velocity of the stage. The step-size between adjacent A-scans can be adjusted by varying the laser PRF and/or speed of the scan-head. For each x-y position, the generated OA responses are recorded at both 532 nm and 578 nm wavelengths. The laser, Pockels cell and data acquisition are synchronized by a programmable pulse generator (PulseBlaster SP17, SpinCore Technologies, Gainesville, USA). In order to correct for per-pulse laser energy fluctuations, a small fraction the laser beam is split off by a beam sampler (BSF10-A, Thorlabs, Newton, USA), detected by a fast, calibrated photodiode (DET10A, Thorlabs, Newton, USA) and digitized by the second channel of the data acquisition card. The photodiode is calibrated prior to imaging by independently measuring the per-pulse energies for both wavelengths at the output of the GRIN lens using a power-meter (J-25MB-LE, Coherent Inc., Santa Clara, USA). The separate A-Scans are then remapped onto a regularly spaced 3D grid using bilinear interpolation.

2.2. Resolution Characterization

The lateral resolution of the hybrid dual-wavelength microscope was characterized in both OA and US modes using sharp edge of a silicon sample which was moved axially across the focus over a range of 2 mm with 100 µm steps. For each z-position, a 3D dataset was recorded and the resolution calculation was performed on the 2D maximum intensity projection (MIP) images, as shown in **Figure 2a**. The resolution analysis further shown in Figure 2b was performed by fitting a sigmoid line-spread function (LSF, red, solid line) to the measured edge response (blue dots). The point-spread-function (PSF, yellow, dashed line) is then calculated as the derivative of the PSF and the resolution is measured as the full width at half maximum (FWHM) of the PSF.
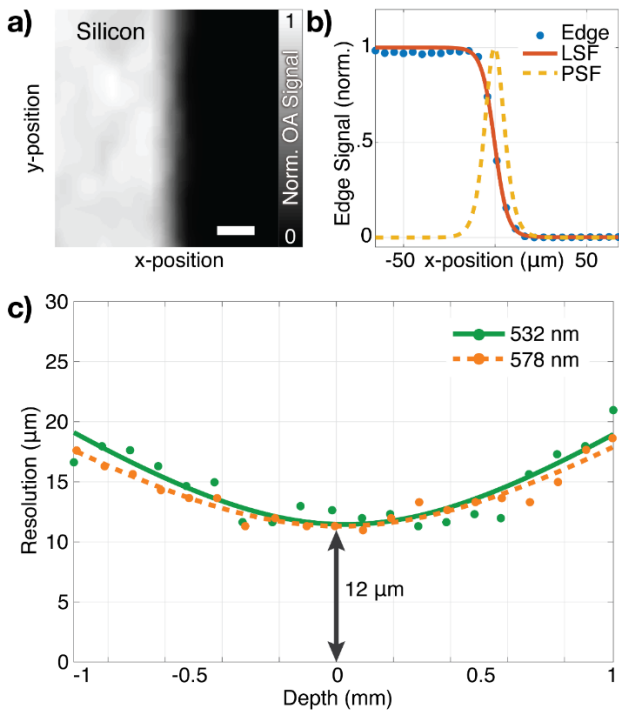
Figure 2 OA resolution characterization using a sharp silicon edge for both 532 nm and 578 nm excitation wavelengths, displaying the long depth of focus of the low-NA gradient index lens. (a) Optoacoustic maximal intensity projection (MIP) image of the silicon edge placed in the optical focus. Scale bar - 10 µm. (b) Resolution characterization based on the full width at half maximum of the point-spread function (PSF, yellow dashed line) calculated as the derivative of the line-spread function (LSF, red solid line) fitted to the recorded OA image of the edge (blue dots). (c) OA imaging resolution as a function of imaging depth, with an in-focus resolution of 12 µm for both 532 nm (green solid line) and 578 nm (orange dashed line).

2.3. Characterization of the Spectral Unmixing Capability

Ink filled tube phantoms were imaged to demonstrate and validate the spectral unmixing capabilities of the system (**Figure 3**). To this end, four crossing polyethylene tubes (outer diameter 500 µm, inner diameter 300 µm) were filled with varying concentrations of blue ink mixed into red ink (both Pelikan, Hannover, Germany), as shown in Figure 3a. The absorption spectra of both inks, as measured by a spectrophotometer (USB4000, Ocean Optics, Dunedin, USA), are shown in Figure 3b. The phantom was then positioned inside a water-filled Petri dish and scanned in both OA and US modes.

2.4. In-Vivo Mouse Imaging

To showcase system's ability to extract both morphological and functional data of complex vascular networks, murine ear and brain were imaged. Six-week-

old female athymic nude-Foxn1nu mice (Harlan Laboratories LTD, Itingen, Switzerland) were used for imaging, in full compliance with European laws on the protection of animals used for scientific purpose and the institutional guidelines of the Helmholtz Center Munich, and with approval from the Government District of Upper Bavaria. Animals were anaesthetized with isoflurane (1.5% to 2.5% v/v) in 100% O_2. Physiological parameters, including blood oxygenation, heart rate, and body temperature were continuously monitored throughout the experiments. The temperature was kept constant using a rectal thermometer and a feedback-controlled heating pad (PhysioSuite, Kent Scientific, Torrington, USA). A custom-designed stereotactic mouse head holder (Narishige International Limited, London, UK) was used to avoid animal motion. The scan head was immersed in a water-filled Petri dish for acoustic coupling and both ear and brain were imaged through a hole in the Petri dish sealed with polyvinylidene chloride foil and using US gel as acoustic coupling medium between the animal and the foil. The mouse ear was fixed to a custom-made mount to ensure a flat topology of the imaged surface. The animal fully recovered within a few minutes after the imaging. The mouse brain was imaged in both OA and US mode with the scalp removed but with the skull intact. The mouse was sacrificed following the brain imaging experiment.

3. Results and Discussion

3.1. Resolution Characterization

The result of the resolution characterization is shown in Figure 2. The small diameter and the long focal distance of the GRIN lens cause a very low NA of 0.025. This NA results in a diffraction-limited lateral resolution in the 11-20 µm range across an extended depth of focus of more than 2 mm. Owing to low NA, the lateral resolution deteriorates by only a factor of $\sqrt{2}$ over a depth range of 2 mm, thus eliminating the need for depth scanning. The axial direction the system's performance is determined by the available US detector bandwidth, effectively translating into an axial resolution of about 44 µm.[16]

3.2. Ink Phantom Imaging

OA images of the ink phantom acquired at 532 nm and 578 nm wavelengths are presented in **Figure 3** along with the US pulse-echo US image and a color photograph of the phantom. Both the red and blue inks have near identical optical absorption at 532 nm, resulting in an equal OA amplitude, as shown in Figure 3a for all the four tubes. In contrast, the absorption of the blue ink is much higher at 578 nm, resulting in an increased OA signal with the increasing blue ink concentrations, as shown in Figure

3b. Using spectral unmixing, we were able to accurately measure the ink concentrations, as displayed in Figure 3e.
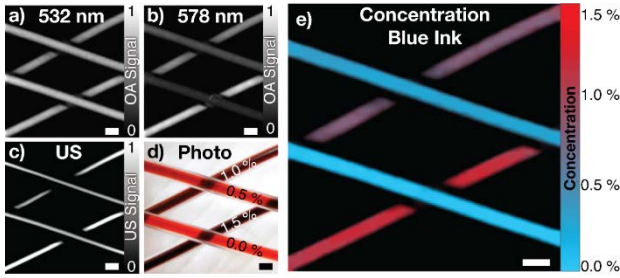

Figure 3 Dual wavelength OA imaging of ink-filled tubes, validating the spectral unmixing capabilities of the system. (a) & (b) OA images recorded at 532 nm and 578 nm, respectively. (c) Corresponding US pulse-echo MIP image. (d) Photo of the ink-filled tubes, indicating concentration of blue ink in the red-blue ink solution. (f) Mapping the blue ink concentration using the dual-wavelength linear unmixing method. Scale bars - 500 µm.

3.3. In-Vivo Imaging

The large-scale imaging capabilities of the system are demonstrated in both **Figure 4 and 5**, showing vascular networks in the murine ear and brain, respectively. Figure 4a displays the vessel-rich network in the ear imaged over a FOV of 3x4 mm² with per pulse laser energy of 1 µJ [22]. Using the dual-wavelength tuning capabilities, the oxygen saturation in the vasculature was further visualized, as shown in Figure 4b. The oxygen saturation map shows typical artery-vein pairs present in the murine ear, with smaller arteries and capillaries providing oxygenated blood to the cells and larger veins removing the deoxygenated blood. The dual-wavelength 3D data acquisition took less than 30 s with a step size of 10 µm and the fast stage moving at an average velocity of 50 mm/s.
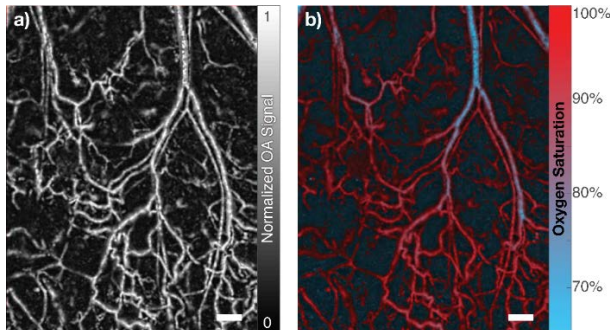

Figure 4 Morphological and functional *in vivo* imaging of a nude mouse ear. (a) Both large arteries and veins as well as fine capillaries can be resolved within the acquired 3x4 mm² field-of-view. (b) Oxygen saturation is further extracted using the dual-wavelength linear unmixing method. Scale bar 300 µm.

Figure 5a shows a depth-encoded MIP of the intricate network formed by vessels both in the skull and the cortex imaged over a large 6x8 mm² area and with the skull intact. Large veins draining into the superior sagittal sinus (SSS) as well as fine pial arteries supplying the cortex with oxygen are clearly resolvable in the image. Figure 5b further displays the corresponding oxygen saturation maps revealing the complex morphology of the highly hypoxic sinusoidal veins located in the skull. [25] The dual-wavelength OA data was recorded within less than 100 s and a with step size of 10 µm whereas the corresponding US scan over the same FOV with a step size of 20 µm was recorded within 30 s.

The naturally co-registered US pulse-echo scan (Figure 5c), recorded prior to the OA dataset, shows precise morphology of the skull, with landmarks such as the separate bone plates and sutures labelled. Note that both volumetric OA and pulse-echo US data were each obtained by a single scan in the lateral plane without the need for additional scanning along the depth dimension, tilling or averaging. Important anatomical landmarks including the crossing of the sagittal and lambdoid sutures (the so-called lambda), as well as the bregma, represented by the crossing between the sagittal and coronal sutures, are easily identified in the US image. The US data may be used to accurately map location of the optoacoustically-recorded vasculature with respect to the skull, which can be subsequently used to correct for skull-induced signal aberrations, thus improving image resolution and contrast and facilitating correct interpretation of the OA data.[26] Finally, the precise skull geometry revealed by the pulse-echo US images may potentially aid in guiding intracranial injections of extrinsic labels and drugs, further minimizing collateral vascular damage. [27]

4. Conclusion & Outlook

A novel hybrid OA and US biomicroscopy approach capable of large-scale morphological and functional brain imaging was realized using dual-wavelength illumination. Rapid wavelength switching in combination with fast mechanical scanning and a flexible, highly sensitive scan head design have enabled the high-speed visualization of both morphology and oxygenation status of large-scale vascular networks with lateral resolution of 12 µm across FOVs covering the entire murine cortex. The flexible scan-head design allows for concurrent high-resolution pulse-echo US scans, providing additional anatomical information.
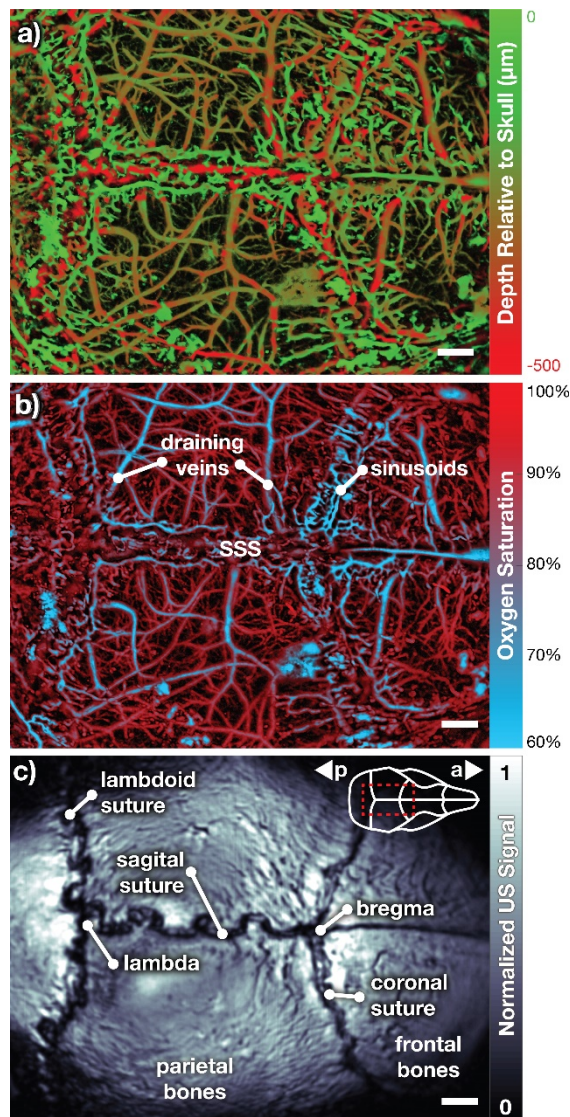
Figure 5 Morphological (a) and functional (b) OA images recorded from cerebral murine vasculature through an intact skull. (c) The co-registered volumetric pulse-echo US image showing the fine skull morphology. Insert in c) displays the approximate location of the field-of-view. Scale bar - 600 µm. SSS - superior sagittal sinus, a - anterior, p – posterior.

The large FOV comes as a trade-off for volumetric imaging speed, which could be inferior to other fast scanning solutions providing smaller FOVs. [18, 21, 23] Nevertheless, the imaging speed is presently limited by the 10 KHz PRF of the laser source. While faster pulsed sources are readily available at 532 nm wavelength, availability of pulsed lasers in the 540-600nm range is limited. Recently, lasers based on stimulated Raman scattering (SRS) in optical fibers have been shown to generate sufficient per-pulse energies in this spectral band,[28, 29] thus can potentially be exploited for accelerating image acquisition with the proposed design.

In conclusion, the presented biomicroscope can bridge the gap between localized microscopic observations and lower-resolution (macroscopic) imaging in whole mouse brains, thus offering a new scalable multimodal tool for investigating healthy and pathological neurovasculature.

References

[1] A. Canazza, L. Minati, C. Boffano, E. Parati, S. Binks, Experimental models of brain ischemia: a review of techniques, magnetic resonance imaging, and investigational cell-based therapies, Frontiers in neurology 5 (2014) 19.

[2] N. Nishida, H. Yano, T. Nishida, T. Kamura, M. Kojiro, Angiogenesis in cancer, Vascular health and risk management 2 (2006) 213.

[3] B.V. Zlokovic, Neurovascular pathways to neurodegeneration in Alzheimer's disease and other disorders, Nature Reviews Neuroscience 12 (2011) 723-738.

[4] A.A. Bogdanov Jr, M. Mazzanti, G. Castillo, E. Bolotin, Protected graft copolymer (PGC) in imaging and therapy: a platform for the delivery of covalently and non-covalently bound drugs, Theranostics 2 (2012) 553.

[5] G.D. Hutchins, M.A. Miller, V.C. Soon, T. Receveur, Small animal PET imaging, ILAR journal 49 (2008) 54-65.

[6] S.R. Meikle, P. Kench, M. Kassiou, R.B. Banati, Small animal SPECT and its place in the matrix of molecular imaging technologies, Physics in medicine and biology 50 (2005) R45.

[7] N.K. Logothetis, What we can do and what we cannot do with fMRI, Nature 453 (2008) 869-878.

[8] R.K. Jain, L.L. Munn, D. Fukumura, Dissecting tumour pathophysiology using intravital microscopy, Nature Reviews Cancer 2 (2002) 266-276.

[9] U. Baran, R.K. Wang, Review of optical coherence tomography based angiography in neuroscience, Neurophotonics 3 (2016) 010902.

[10] E. Macé, G. Montaldo, I. Cohen, M. Baulac, M. Fink, M. Tanter, Functional ultrasound imaging of the brain, Nature methods 8 (2011) 662-664.

[11] P. Beard, Biomedical photoacoustic imaging, Interface focus (2011).

[12] A. Taruttis, V. Ntziachristos, Advances in real-time multispectral optoacoustic imaging and its applications, Nat Photonics 9 (2015) 219-227.

[13] X.L. Deán-Ben, G. Sela, A. Lauri, M. Kneipp, V. Ntziachristos, G.G. Westmeyer, S. Shoham, D. Razansky, Functional optoacoustic neuro-tomography for scalable whole-brain monitoring of calcium indicators, Light: Science & Applications 5 (2016) e16201.

[14] X. Luís Deán-Ben, D. Razansky, Adding fifth dimension to optoacoustic imaging: volumetric time-resolved spectrally enriched tomography, Light: Science & Applications 3 (2014).

[15] D. Wang, Y. Wu, J. Xia, Review on photoacoustic imaging of the brain using nanoprobes, Neurophotonics 3 (2016) 010901-010901.

[16] H. Estrada, J. Turner, M. Kneipp, D. Razansky, Real-time optoacoustic brain microscopy with hybrid optical and acoustic resolution, Laser Physics Letters 11 (2014) 45601.

[17] H.F. Zhang, K. Maslov, M. Sivaramakrishnan, G. Stoica, L.H.V. Wang, Imaging of hemoglobin oxygen saturation variations in single vessels in vivo using photoacoustic microscopy, Applied Physics Letters 90 (2007) 53901.

[18] B. Ning, N. Sun, R. Cao, R. Chen, K. Kirk Shung, J.A. Hossack, J.M. Lee, Q. Zhou, S. Hu, Ultrasound-aided Multi-parametric Photoacoustic Microscopy of the Mouse Brain, Sci Rep 5 (2015) 18775.

[19] L. Wang, K. Maslov, J. Yao, B. Rao, L.V. Wang, Fast voice-coil scanning optical-resolution photoacoustic microscopy, Opt Lett 36 (2011) 139-141.

[20] B. Ning, M.J. Kennedy, A.J. Dixon, N. Sun, R. Cao, B.T. Soetikno, R. Chen, Q. Zhou, K.K. Shung, J.A. Hossack, Simultaneous photoacoustic microscopy of microvascular anatomy, oxygen saturation, and blood flow, Optics letters 40 (2015) 910-913.

[21] J. Yao, L. Wang, J.M. Yang, K.I. Maslov, T.T. Wong, L. Li, C.H. Huang, J. Zou, L.V. Wang, High-speed label-free functional photoacoustic microscopy of mouse brain in action, Nat Methods 12 (2015) 407-410.

[22] American National Standard for Safe Use of Lasers in Health Care Facilities. Standard Z136.1, 2014.

[23] J.Y. Kim, C. Lee, K. Park, S. Han, C. Kim, High-speed and high-SNR photoacoustic microscopy based on a galvanometer mirror in non-conducting liquid, Scientific reports 6 (2016) 34803.

[24] S. Gottschalk, T. Felix Fehm, X. Luís Deán-Ben, D. Razansky, Noninvasive real-time visualization of multiple cerebral hemodynamic parameters in whole mouse brains using five-dimensional optoacoustic tomography, Journal of Cerebral Blood Flow & Metabolism 35 (2015) 531-535.

[25] S. Sakadžić, E. Roussakis, M.A. Yaseen, E.T. Mandeville, V.J. Srinivasan, K. Arai, S. Ruvinskaya, A. Devor, E.H. Lo, S.A. Vinogradov, Two-photon high-resolution measurement of partial pressure of oxygen in cerebral vasculature and tissue, Nature methods 7 (2010) 755.

[26] H. Estrada, X. Huang, J. Rebling, M. Zwack, S. Gottschalk, D. Razansky, Virtual craniotomy for high-resolution optoacoustic brain microscopy, Scientific reports 8 (2018) 1459.

[27] R.L. Lowery, A.K. Majewska, Intracranial injection of adeno-associated viral vectors, Journal of visualized experiments: JoVE (2010).

[28] Y. Liang, L. Jin, B.-O. Guan, L. Wang, 2 MHz multi-wavelength pulsed laser for functional photoacoustic microscopy, Optics letters 42 (2017) 1452-1455.

[29] P. Hajireza, A. Forbrich, R. Zemp, In-vivo functional optical-resolution photoacoustic microscopy with stimulated Raman scattering fiber-laser source, Biomedical optics express 5 (2014) 539-546.

Graphical Abstract for Table of Contents

Text: Diseases affecting neurological function are often linked to pathological changes in the neurovasculature. Efficient visualization of the complex neurovasculature network is hindered with the existing optical microscopy techniques due to sub-optimal trade-offs between the spatiotemporal resolution, field-of-view and type of contrast. We present a hybrid optoacoustic-ultrasound biomicroscope capable of fast transcranial morpho-functional imaging of the entire murine cerebrovascular network. The new approach holds promise to greatly facilitate studies into neurological and vascular abnormalities of the brain.

Image:

Large-Scale Morpho-Functional Optoacoustic and Ultrasound Biomicroscopy